

Point Source sensitivity, Pupil alignment, Calibration and Control for TMT-NFIRAOS-IRIS¹

Glen Herriot^a, Jean-Pierre Véran^a, Olivier Lardière^a, Ryuji Suzuki^b, Gelys Trancho^c
^aNational Research Council Canada, ^bNAOJ, ^cTMT

ABSTRACT

We present details of end-to-end procedures, algorithms, test equipment and performance budgets for pupil alignment, during commissioning and on-sky during observing for first light adaptive optics on TMT. A surprisingly large 30% observing time penalty would arise from only 1% end-to-end pupil misalignment between the primary mirror of the Thirty Meter Telescope and the Lyot stop in IRIS, the first light client instrument for NFIRAOS. This penalty results from undersizing the Lyot stop to block background light, on a misaligned pupil, which reduces throughput and more importantly degrades PSF. On-sky, NFIRAOS will feed back image position, wavefront error and pupil shift error signals to the telescope control system to adjust the alignment of TMT's three mirrors, but this is only possible after careful calibration. We describe specialized test equipment that includes pupil viewing cameras and a high resolution WFS patrolling each output port to assess pupil position. The WFS stage runout would confound measurements, but is self-calibrated by reference sources and by poking DM actuators. Finally we discuss the mechanical compensation strategy consisting of shimming instruments and pointing NFIRAOS' instrument selection fold mirror, and motorized recentering of an instrument Lyot stop on the as-built beam using its pupil viewing camera also referenced to DM actuator pokes. As a result we expect to achieve a more tolerable but still significant 12.5% loss of observing efficiency from pupil misalignment.

1. INTRODUCTION

The sensitivity advantage of a telescope with perfect Adaptive Optics increases with D^4 , where D is the diameter of the telescope primary mirror. This sensitivity is the product of primary mirror area increasing as D^2 , and the reciprocal of the area of the point spread function (PSF), also increasing with D^2 . However, this theoretical advantage is degraded by multiple real-world factors including among others optical throughput, thermal background and residual wavefront error. This latter degrades sensitivity by a factor proportional to S^2 , where S is the Strehl ratio of the image.

Traditional approaches to optimize AO-corrected sensitivity are: to increase the Strehl ratio; to optimize optical throughput by means of high quality optical coatings, reduction of number of surfaces, and building and operating an instrument in a clean environment. Efforts to reduce thermal background also involve fewer optical surfaces, with good coatings, and cold Lyot stops in instruments. And as is well-known, NFIRAOS the adaptive optics system for the Thirty Meter Telescope (TMT) will be cooled to -30 C, which dramatically reduces exposure time by 2.5x for K-band spectroscopy. Finally reducing stray light and ghosts by wedging beam-splitters, and using baffles could potentially be valuable.

2. POINT SOURCE SENSITIVITY

Point Source Sensitivity is proportional to the inverse of observing time for imaging unresolved point sources with noise principally due to background.

$$\text{PSS} \propto \frac{A}{f_{bg}} \int \varphi_{(\theta)}^2 d\Omega \quad (1)$$

¹ TMT.AOS.TEC.17.165

Where $\varphi_{(\theta)}$ is the 2D PSF profile normalized so that $\int \varphi_{(\theta)} d\Omega = 1$, A is the telescope aperture area, and f_{bg} is photon flux of background per unit area, unit time, and unit solid angle. However, Point Source Sensitivity is most useful when Normalized to a reference case, and is then called PSSN.

$$\text{PSSN} = \frac{A}{A_0} \times \frac{f_{bg0}}{f_{bg}} \times \frac{\int \varphi_{(\theta)}^2 d\Omega}{\int \varphi_{0(\theta)}^2 d\Omega} \times \dots \quad (2)$$

In equation (2), A_0 is the telescope aperture as designed, unvignetted by a Lyot stop, f_{bg0} is the sky and telescope background with a perfectly aligned and sized Lyot stop, and $\varphi_{0(\theta)}$ is the diffraction limited PSF.

Other factors multiply with those in (2), as listed in the PSSN budget in the next section.

3. POINT SOURCE SENSITIVITY NORMALIZED BUDGET

This budget is for background-limited imaging of unresolved point sources. Numbers in the PSSN budget in Table 1 multiply together. If each item in the PSSN budget were perfect, it would be equal 1.0. However, the various terms in the second column of Table 1 together result in PSSN= 0.161, meaning that it takes approximately 7x more exposure time to detect a point source than for a TMT built to its nominal design, with 100% throughput and perfect AO correction. Items in the second column are themselves the products of terms in the third column. We describe these in turn.

High order wavefront error of 172 nm from the NFIRAOS wavefront error budget causes a PSSN factor proportion to Strehl Ratio squared [[3]], which we estimate via the Marechal approximation. Low order wavefront error (tip, tilt, focus & astigmatism), as mentioned previously, reduces sensitivity proportional to Strehl ratio, because it only causes a slight broadening of the PSF core, and does not throw light a long way from the core.

Table 1 AO normalized point source sensitivity imaging budget for TMT NFIRAOS IRIS

Item	On Axis PSSN Budget	
	K	
PSSN MCAO NFIRAOS + IRIS Imager	0.161	
Wavefront Error (PSS $\propto S^2$)	0.592	
High Order WFE in nm -> S ²		0.617
Lo Order WFE broadening PSF -> S		0.960
Throughput (PSS $\propto \eta$)	0.328	
Telescope Requirement		0.910
NFIRAOS Requirement		0.800
IRIS Imager Requirement		0.450
Pupil Shift (0.4% Undersized Lyot)	0.875	
Undersized IRIS Lyot mask vignetting		0.955
Undersized Lyot mask PSF broadening		0.917
Background [PSS $\propto (1+I_p/I_0)^{-1}$]	0.958	
Thermal Background		0.960
Scattered Light		0.999
Out of focus ghosts		0.999
Image Smearing (PSS $\propto S$)	0.997	
Image derotator		
Offset b/w OIWFS/IRIS Focal plane		
ADC errors		
Amplitude non-uniformities	0.994	
Atmospheric scintillation		0.994
M1 segments T.P variation		0.9998
Ghosting (PSS $\propto 1-2\epsilon$)	0.999	
Static focused ghost $<5 \times 10^{-4}$		0.9995

Throughput items are taken verbatim from top-level observatory requirements for TMT, NFIRAOS and its first-light client instrument IRIS, and directly enter the PSSN budget as values equal to the throughput requirements.

Pupil Shift is the major focus of this paper and contains two components: direct throughput loss from a Lyot mask; and PSF broadening. It is derived from a bottom-up misalignment estimate of 0.4% in section 5, Pupil Shift Budget and converted to PSSN by methods described in section 4.

Background effect on PSSN.

$$\text{PSSN} = \frac{1}{1 + \frac{f_{bg}}{f_{bg0}}} \quad (3)$$

NFIRAOS is required to not increase the background from the sky and telescope by more than 15% in the inter-OH gaps for the purpose of spectroscopy sensitivity. For that reason NFIRAOS is cooled to -30C.

NFIRAOS design requirements specify that NFIRAOS shall have sufficient baffling to reduce stray light to levels such that any image degradation resulting from light originating outside the 120 arcsecond technical field is less than 0.999-point source sensitivity. However, in light of the other much more significant terms in the PSSN budget, this number is stringent and may be rebalanced in future. For similar reasons, NFIRAOS does not use a Narcissus mirror on the ‘fourth port’ of the beamsplitter since the payoff would be very minor. However the science beamsplitter does have good anti-reflection coatings and a 10 to 40 arcsec wedge to ensure that NFIRAOS static focused ghost is less than 5×10^{-4} and shifts these defocus ghost images just outside the control radius of the AO system, $\lambda/(2D/60)$.

Image smearing is specified in the TMT Observatory Requirements to be <0.5 mas, and is caused by errors in the image rotator, slow speed tracking and guiding errors, flexure of On-instrument WFS (OIWFS) w.r.t. science detector, and differential errors between science and OIWFS ADCs due to design, control and catalog colour errors. It is converted to PSSN in [[3]].

4. RELATIONSHIP OF PSSN TO PUPIL ALIGNMENT

Until recently a very important item, the impact of pupil alignment, has been overlooked. A 1% end-to-end pupil misalignment would cause a 30% observing time penalty, i.e. reduction in PSSN by 30%. This surprising effect arises because if the telescope pupil is expected to be misaligned onto an instrument Lyot stop due to tolerances, then the Lyot stop should be undersized to block background light. This is the situation originally proposed for TMT NFIRAOS and its first-light client instrument IRIS, an imaging spectrograph, shown on the left of Figure 2. How did we originally select 1% undersizing? A decade ago we decided to do “twice as good as Gemini for Lyot masks undersizing.” Furthermore, it is challenging for the Telescope to steer its pupil accurately onto DM0 within NFIRAOS, which has a goal to work with D/240 pupil shift on DM0, otherwise it increases tomography errors. NFIRAOS wavefront error budget allocates 12 nm for tomography effects due to 1/240 pupil shift. This is split equally in quadrature among the telescope control system, M2 and M3 actuators, and measurement errors by NFIRAOS.

In what follows we define a pupil undersizing factor $\alpha = 2 \times \text{shift}$. I.e. if the worst case pupil misalignment is foreseen to be $\pm 1\%$ of the pupil diameter, then $\alpha = 0.02$. When designing a Lyot mask, all interior edges intrude into the aperture by $\alpha = 2 \times \text{shift}$. The mask’s serrated outer perimeter is shrunk by αD ; the central obscuration is enlarged by αD ; and the M2 spider widths are thickened by αD . See Figure 2. Thus, starting from a pupil mis-centring of 1%, the area losses alone would be 11%. But this area loss is not the major effect.

In addition to throughput losses from reduced pupil area of a Lyot mask designed for expected tolerances, a bigger loss is that the smaller and less-filled pupil creates an image with a broadened PSF. *PSF* $\varphi(\bar{\theta})$ is the squared absolute value of the Fourier transform of the pupil function $P_{tel(\bar{\rho})}$ vignetted by the Lyot stop $T_{LS(\bar{\rho},\alpha,\beta)}$; (β is as-built pupil shift).

$$\varphi(\bar{\theta}) = \left| \text{FT} \left[\frac{P_{tel(\bar{\rho})} T_{LS(\bar{\rho},\alpha,\beta)}}{\int P_{tel(\bar{\rho})} T_{LS(\bar{\rho},\alpha,\beta)} d\bar{\rho}} \right] \right|^2 \quad (4)$$

Thus relative to the primary mirror pupil, the Strehl ratio is decreased, which affects PSSN proportional to S^2 . For 1% pupil shift on TMT, PSF broadening would cause another 21% loss of observing time, for a total of 30% losses with an undersizing factor $\alpha = 2 \%$, as shown in Figure 1. Clearly this is a very big penalty, and we have worked hard to reduce

this effect down to our current bottom-up estimate of the necessary stop undersizing of a 0.4% pupil shift, or $\alpha=0.08$. This shift is derived a bottom-up budget in Table 2 and then the sensitivities shown Figure 2 are applied to create the two pupil shift entries in the PSSN budget of Table 1. The End-to-end alignment of M1 pupil onto Lyot stop in Table 2 is for residual errors after employing the strategies and equipment described from section 6 to the end of this paper.

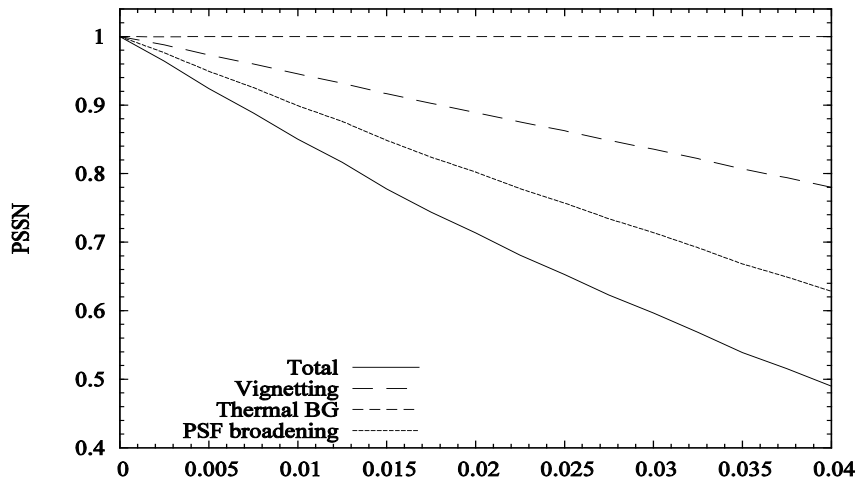


Figure 1 Mask undersizing loss factor α (fraction of diameter)

5. END TO END PUPIL SHIFT BUDGET M1 TO IRIS LYOT STOP

Table 2 contains the bottoms up budget for the residual misalignment of the pupil on to IRIS' Lyot stop. Blurring of the Pupil on IRIS Lyot stop due to IRIS optical design is a systematic error that has been analyzed in Zemax by Ryuji Suzuki at 0.2% and is the largest single item in the budget. Mechanical design guidelines for IRIS random errors are to use 2-sigma tolerances for a total of two times the RMS pupil misalignment, so the top line of the budget is the systematic errors plus double the second line which is the quadrature sum of the random errors in the lines below and to the right.

The NFIRAOS portion of the estimate has six items. The first is the accuracy of the pupil steering mirror in the Pyramid WFS within NFIRAOS. If it is wrongly positioned, then measurements of pupil centroid on the PWFS CCD will be in error. Its zero-point will be calibrated using DM pokes in the daytime, but at night this accuracy will corrupt feedback to the telescope control system. The pupil steering mirror depicted in Figure 7 has a specified mechanical accuracy of 10 micro-radians, and an optical sensitivity of $2/67$ of the pupil diameter for each milli-Radian of tilt.

In addition, the pupil position on the PWFS detector is determined by the quality of the pointing model that drives motors for X, Y, Focus and ADC stages as the PWFS patrols the field to select a guide star.

Image centroiding error on the PWFS detector is given for a circular matched filter, in bright time, (the usual NFIRAOS observing scenario), where sky background actually helps to reduce measurement errors. This is described also in Section 6.2 Pupil Centroiding.

The primary mirror (M1) segment reflectivity varies due to a recoating schedule with a 2 year cycle. Degradation between recoating is expected to be 6%, and slightly affects matched filter centroiding. The plan to coat ~1% of the segments each week, results in a rectangular probability distribution of segment reflectivity, which the matched filter is nearly immune to.[1]

The exit pupil diameter from NFIRAOS has an uncertainty because of the variation of the f/number ($f15 \pm 0.01$), due to focal length tolerances of the OAPs in the science path, resulting in a NFIRAOS pupil magnification error of $0.067\% = 0.01/15$. However on-sky, the magnification is tightly controlled by IRIS' on-instrument WFSs, typically deployed in a triangle enclosed by a circle of ~60 asec diameter, each with a tolerance of 2 mas RMS, resulting in $0.006\% = \sqrt{3} \cdot 2/60$ pupil magnification uncertainty. Its axial tolerance will also blur NFIRAOS' exit pupil on the Lyot stop.

How well the telescope can respond to feedback from NFIRAOS and repoint the pupil is limited by the tertiary mirror M3 pointing accuracy (see section 4.2 of TMT.AOS.TEC.15.103.DRF01).

Table 2 End to end alignment of M1 pupil onto Lyot stop

Item	Undersizing IRIS Lyot Mask			
Mask Undersize (Systematic + 2 * random)	0.40%			
Systematic errors		0.20%		
IRIS Optical Blurring of Pupil (systematic)			0.20%	
Random errors RMS sum (1 sigma)		0.10%		
NFIRAOS			0.05%	
Pupil mirror in PWFS - accuracy				0.030%
Pointing model errors for PWFS				0.030%
Pupil image centroiding				0.010%
M1 segment non-uniformity				0.005%
NFIRAOS exit pupil magnification				0.006%
Axial Tolerance of Exit pupil				0.025%
Telescope (M3)			0.002%	
RSS of IRIS random terms			0.050%	
Rotating Offset center of mass of cryostat/OIWFS				0.028%
Accuracy of XY stage for Lyot stop				0.026%
Fabrication accuracy of Lyot stop				0.005%
Position error of the Lyot stop in Z direction				0.001%
NFIRAOS Simulator Pupil position error in Z direction				0.012%
DM11 poke pattern meas. error				0.017%
Centroiding Mask on PV vs poke pattern				0.010%
Adjustment error of the tilt ring				0.022%
High frequency rotator bearing runout				0.006%
Global Contingency			0.070%	

The last half of the table shows the IRIS random terms 1-sigma total; this quadrature sum is doubled for inclusion the top level of the table. The first IRIS item is the uncorrectable wander of the optical axis because its rotating centre of mass is not concentric with its bearing and trusses. Deploying the stop after homing its stages will have a mechanical error in the XY stage of 50 micron 2-sigma. Manufacturing accuracy of Lyot stop (0.1 mm tolerance on 100 mm diameter aperture) means that it must be slightly undersized.

The next line shows the axial installation accuracy of the Lyot mask after internal IRIS measurements. These depend on a ‘NFIRAOS Simulator’ prior to mating IRIS to NFIRAOS, and the simulator will have axial errors.

On NFIRAOS, by poking a sparse pattern on the high altitude DM11, Talbot propagation to the Lyot stop will create a pattern of intensity spots on the pupil viewing camera within IRIS. We estimate that the overall pattern may be centroided to 1% of a spot pitch via a correlation algorithm to establish where the pupil is on IRIS’ pupil viewing camera. However, additionally, there are pupil camera measurement errors in determining the offset of the mask silhouette w.r.t. this poke pattern

The next line “Adjustment error of the tilt ring” is an allowance for the planned instrument rotator bearing alignment procedures. The rotator-dependent wander of the pupil location is measured with the pupil viewing camera. Then a cylindrical wedge shim (tilt ring), between the science dewar and the rotor of the bearing, is clocked to minimize angular runout. This runout is due to the intrinsic bearing runout, as well angular wobble caused by rotating an unbalanced dewar centre of gravity, which flexes the instrument support trusses. The tilt ring can be bolted in discrete rotations giving 50 uRad angular steps, divided by sqrt(12) for quantizing noise, and scaled by the 200 m lever arm from the focal plane to the NFIRAOS exit pupil. The IRIS team studied and discarded an alternative scheme to build a pointing model of this angular runout and use it to drive the mask XY stage continuously during observations with this same generous error allocation. In the chosen method, the XY stage is used only during off-line alignment – the mask remains stationary w.r.t. the IRIS optics after calibration .

Nonetheless, high angular frequency IRIS rotator bearing angular runout (50 um pk-valley over 2 m radius) will remain. We assume 1/3 is uncorrectable high frequency residual. Finally we include contingency to bring the total to 0.4% of Diameter for pupil mis-pointing and related effects like blurring.

6. CALIBRATION AND ALIGNMENT PROCEDURES

6.1 Pupil and Image rotation and shift

On the left hand side of Figure 2, are NFIRAOS and client instruments, with IRIS on the bottom port. Light from the telescope enters the window at centre-left in this image. Because TMT is an Alt-Az design, and NFIRAOS sights at 5.5 degrees from the elevation axis of the telescope, the image rotates on the input focal plane delivered into NFIRAOS, and also the pupil rotates on the ground-conjugated DM at a rate that is slightly non-linear function of elevation angle. Each instrument has a derotator to track image rotation, and also reimages the pupil onto a rotating undersized Lyot mask.

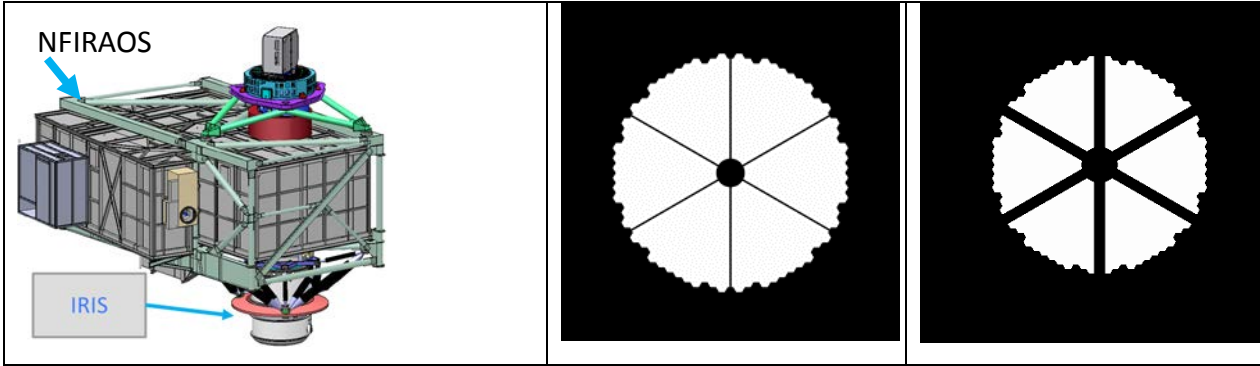


Figure 2 Left: NFIRAOS and its client instruments; Centre: TMT pupil; Right Lyot mask undersized by $\alpha = 2 \times$ shift on on all interior edges for a 1% pupil misalignment shift.

Inside NFIRAOS, the Truth (Pyramid) WFS travels in a circular path on an XY stage to track a natural guide star in the rotating field of view. Meanwhile the four pupil images on the PWFS detector each have a rotating view of the telescope spiders. The NFIRAOS Real Time Computer centroids the pupil [1], and feeds its XY position back to the telescope control system to repoint its tertiary mirror and/or secondary mirror in a coordinated motion to steer the pupil while maintaining image position and minimizing field dependent aberrations. As shown in Figure 4, this feedback stabilizes the first leg of the path (M1 to DM0) from the telescope pupil to IRIS' Lyot stop. The second leg from DM0 to the interface between NFIRAOS and IRIS, will be calibrated using a test instrument NSEN, described below. Finally, the last leg is the pupil shift occurring between the instrument interface and the Lyot stop within the instrument, calibrated with a pupil viewing camera in IRIS.

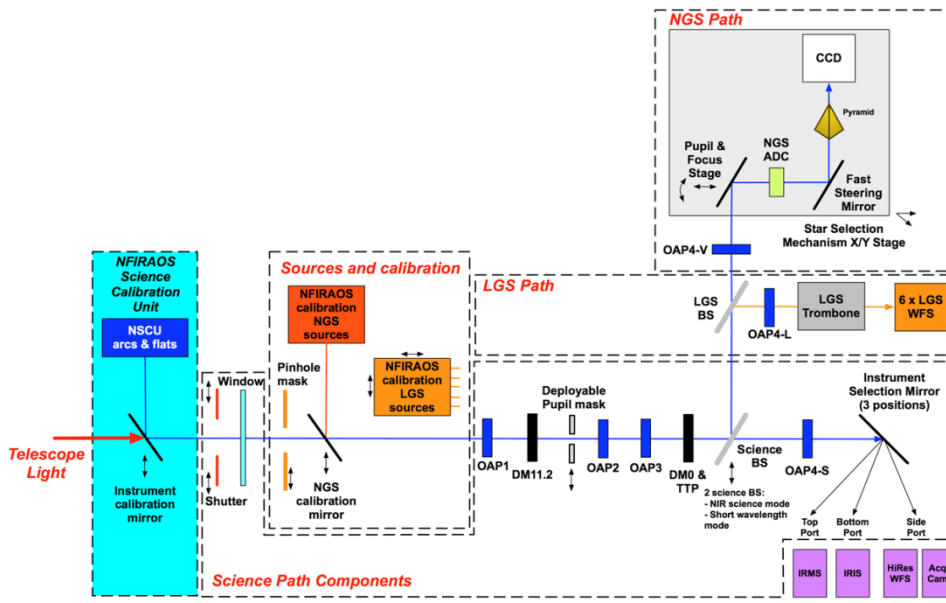
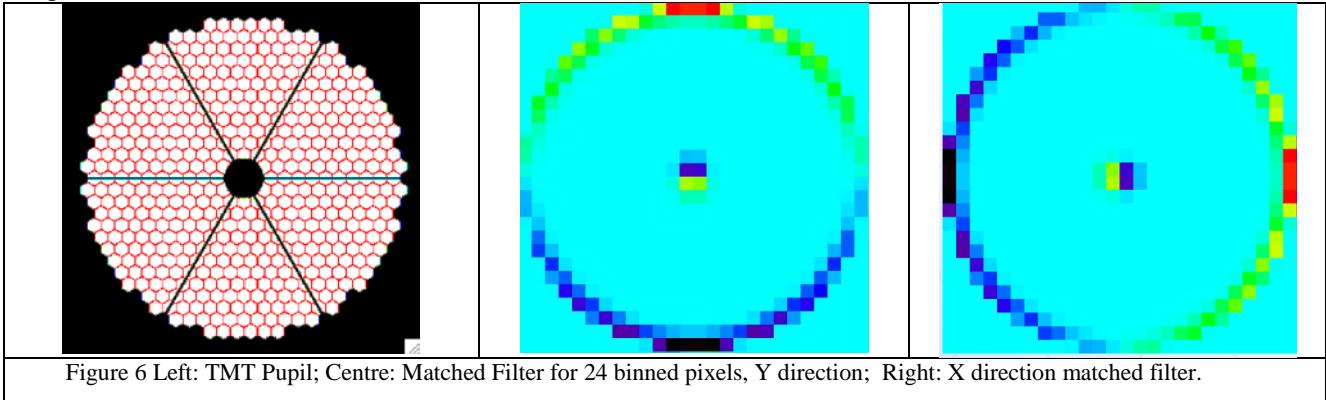


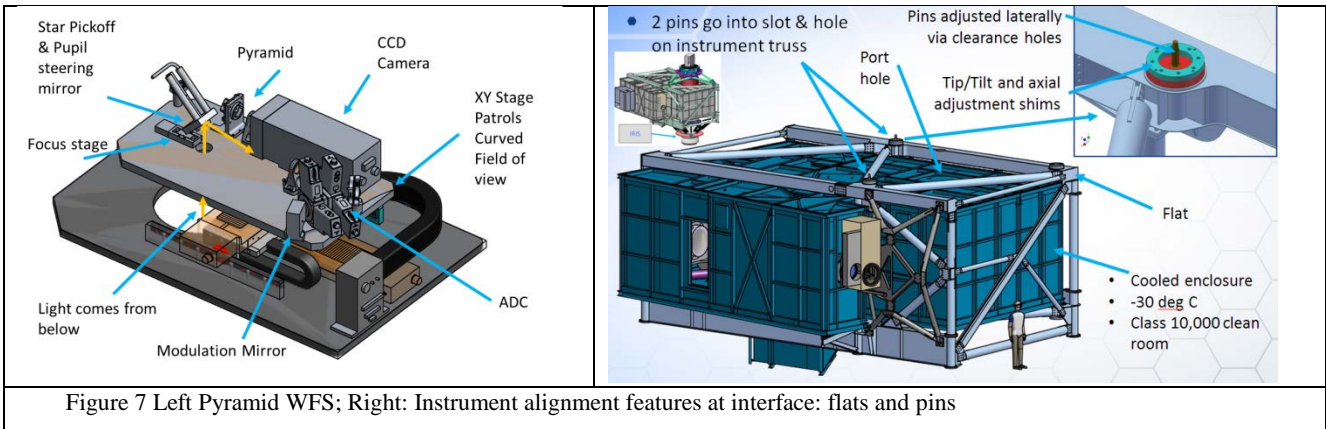
Figure 3 Science path is blue horizontal line running left to right.

Figure 6 shows the X and Y matched filters derived for a binned 24x24 pupil image. The binned image and each matched filter are rasterized into vectors. The dot product of a matched filter vector and the image vector gives the pupil displacement measurement.



6.3 Repeatable Instrument Mounting Interface

Each NFIRAOS Client instruments is attached by trusses that engage three pads that define a mounting plane. (Datum E in Figure 11) Two of these pads also have tapered alignment pins that define the location of the output light beam. We will survey (using NSEN, described below) and adjust these pins laterally in-plane, and shim the pad thickness to locate the instrument mounting plane at the required distance and angle tolerance from the focal plane (and exit pupil).



6.4 NSEN

During commissioning of NFIRAOS, and up until the time that an eventual third instrument is installed on it, there will be a piece of test equipment NSEN, on an unused port. NSEN has an acquisition camera to help TMT locate the brightest guide star. But NSEN also on the same XYZ stage has a high resolution (120 x 120) Shack-Hartmann WFS used for diagnostics and non-common-path calibration. The NSEN HRWFS also has an important role in surveying the exit beam location and pupil location to permit adjusting the instrument interface pads and pins. The left hand cartoon in Figure 8 depicts a cross section of NSEN and its HRWFS on an XYZ stage. The problem is that it is in a cooled enclosure, supported by trusses, just like an instrument. So the actual location and tilt of the stage is uncertain with respect to the instrument interface pads and pins. First we calibrate the flatness of the stage travel due stage runout by measuring the XY location errors of a row or column of pinholes and integrate along the path to compute the stage flatness (i.e. similar algorithm to CureD).

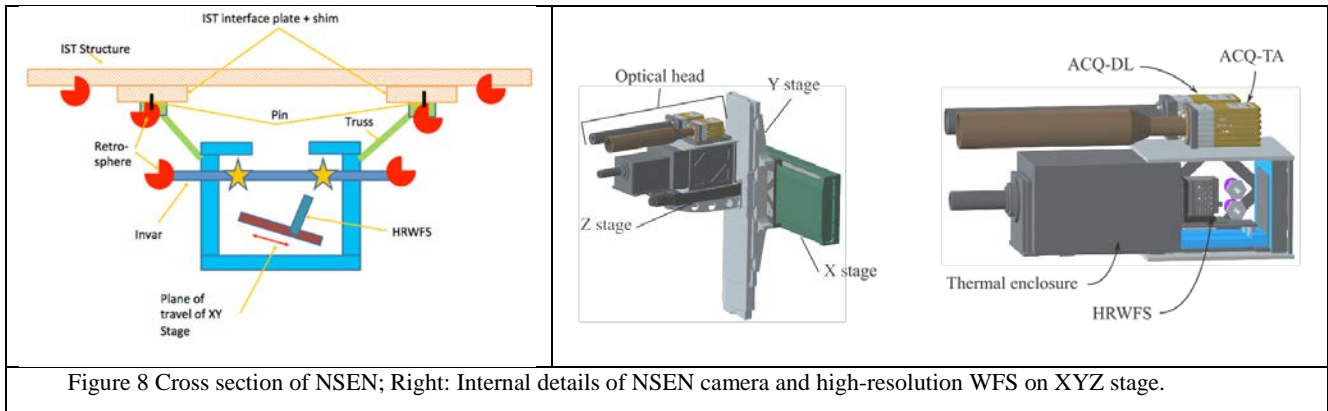


Figure 8 Cross section of NSEN; Right: Internal details of NSEN camera and high-resolution WFS on XYZ stage.

To calibrate the global tip/tilt/piston of the plane of travel of the HRWFS, there are three point sources located in the nominal focal plane, just outside the 2 arcminute field of view of the NFIRAOS output beam. These sources (shown as stars in Figure 9 right) are arranged in a triangle and supported by a low thermal expansion frame (e.g. Invar or Zerodur). This frame has extensions outside the NSEN thermal enclosure, which hold retrospheres. Prior to assembly of NSEN, the relationship of the point sources to the spheres will be measured accurately with a coordinate measuring machine. Later, when NSEN is mounted on NFIRAOS, laser tracker distance measuring devices (e.g. Faro or Leica) will measure the plane of the spheres with respect to the instrument interface. Then by visiting and focusing the HRWFS on the three calibration point sources, we will know where the HRWFS focal plane is w.r.t. the instrument interface.

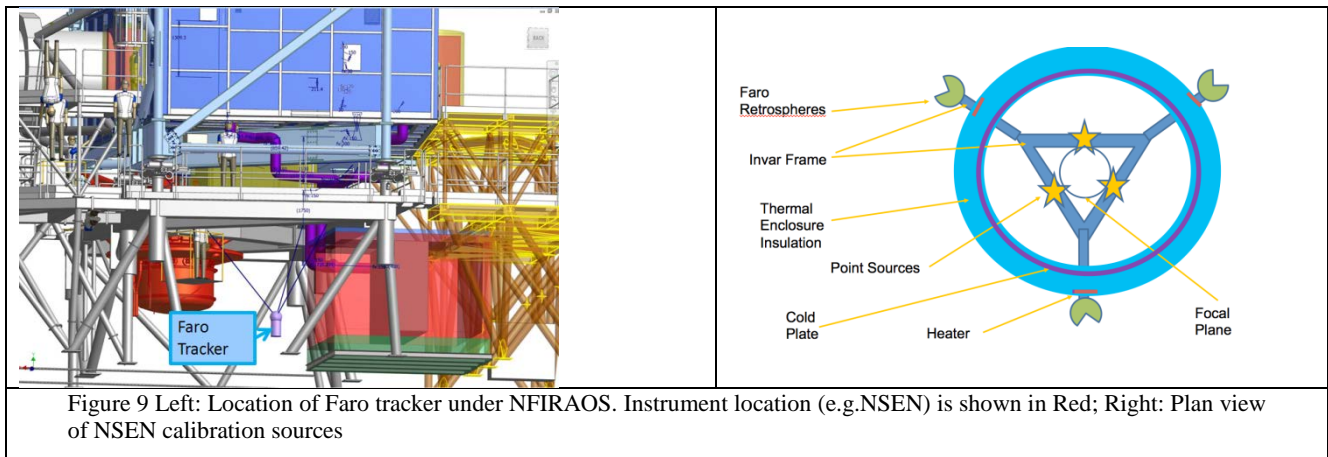


Figure 9 Left: Location of Faro tracker under NFIRAOS. Instrument location (e.g.NSEN) is shown in Red; Right: Plan view of NSEN calibration sources

Finally, the HRWFS will patrol the focal plane, measuring in tip/tilt and focus a grid of pinholes from the very accurate source simulator focal plane mask. A least squares fit of the tip/tilt and focus WFS measurements will estimate the centre of curvature of the delivered focal plane (C in Figure 10, along with the centre (A) of the pinhole grid image. The line joining A & C should be normal to the interface plane as transferred via the metrology chain from the retro spheres and NSEN point sources.

As well, the centre of the pinhole grid should be at the centre of a fixed diameter theoretical circle passing through the two instrument locating pins. Otherwise, the instrument locating pins and pads must be translated and shimmed respectively to achieve the tolerances shown in Figure 11. In addition, the instrument selection fold mirror can be steered remotely to help move the image. Residual tilt of the focal plane is equivalent to having the pupil off-centre. These tolerances are a good start towards delivering the pupil in the right place within IRIS, but are not by themselves sufficient to permit using an acceptably undersized Lyot mask.

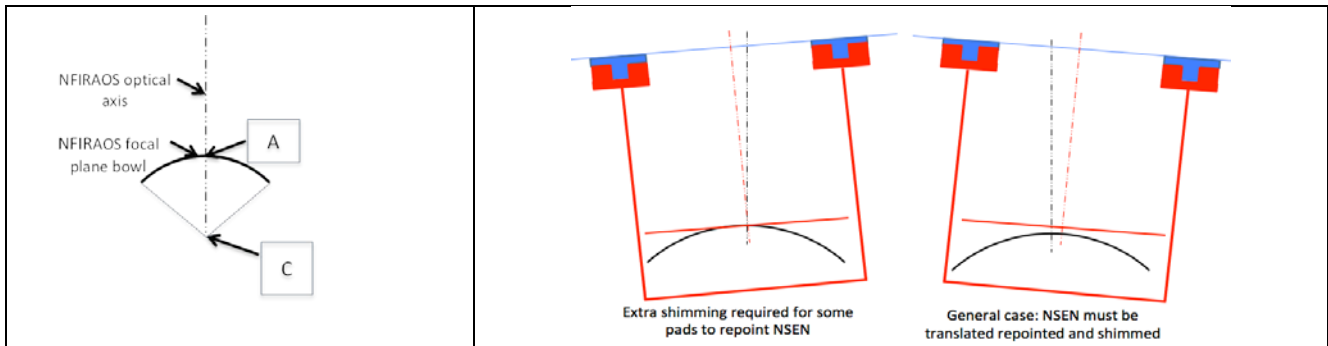


Figure 10 Left: Fully aligned condition. A is image of source simulator focal plane mask central pinhole (Figure 5), and C is centre of curvature of focal plane bowl. A & C should be centralized and on a line normal to the plane of the mounting pads. Center: Interface is centered, but tilted. Right: Pad thickness should be shimmed, and pins translated.

IRIS Imaging Spectrograph

The first light instrument for NFIRAOS will be IRIS. An optical block diagram of IRIS is on the right of Figure 11, highlighting two key features: a rotating pupil mask on an XY stage, and a deployable pupil viewing camera. The pupil mask design, together with the prototype of the rotation stage is shown in Figure 12.

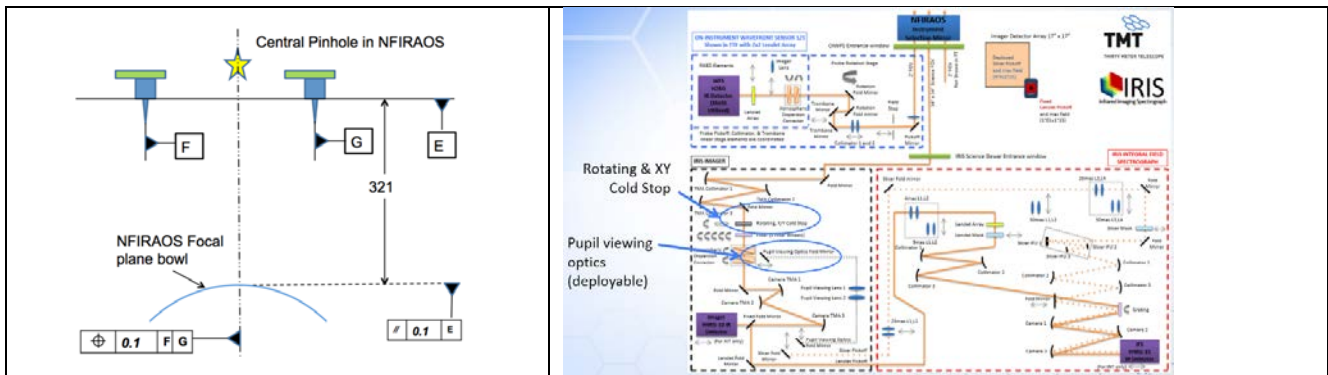
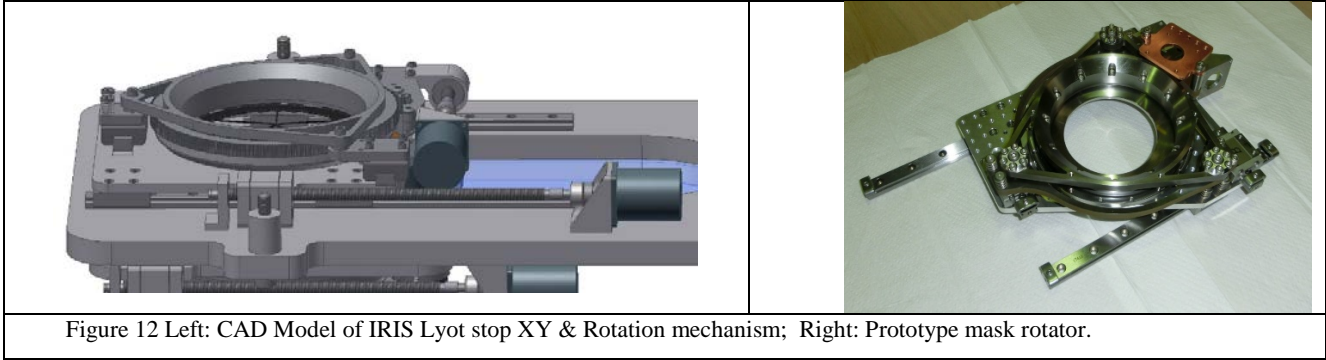


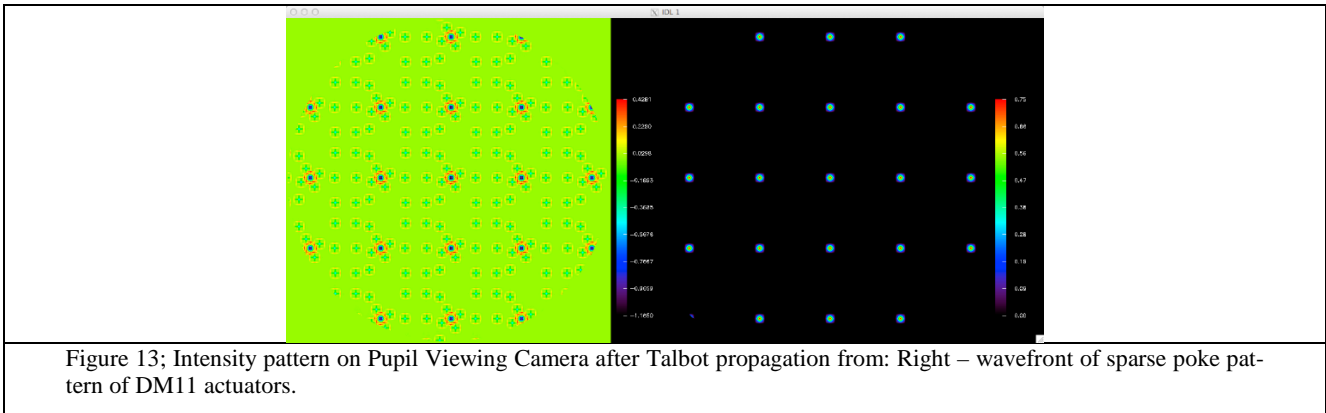
Figure 11 Left: Alignment tolerances after measurement and adjusting. Datum E is the plane of the mounting pads, and the optical axis is the centre of a 6.1 m diameter theoretical circle passing through the pins, Datum F & G. Right IRIS Imaging Spectrograph.

During astronomical observations, as shown in Figure 4, the image from the telescope rotates when received by NFIRAOS, and each of NFIRAOS' client instruments have their own rotator to compensate. Angular runout on IRIS rotator bearing would cause IRIS optical axis to precess and tilt as it tracks sky rotation. As mentioned previously, a tilt on the focal plane appears as a pupil shift on the Lyot stop. During initial alignment, the IRIS team will adjust a circular wedge shim located between its rotator bearing and its science cryostat to compensate.

As well, the best XY position of the Lyot stop will be measured and set into position, and not moved during observations, although the Lyot stop rotation stage will rotate, albeit at a different rate than the main instrument rotator. To determine the best XY location of the Lyot stop is a two-step process. First a rough alignment will be determined with the pupil viewing camera, while scanning the XY stage to locate the edges of the oversized pupil stop at the ground conjugated DM0, when illuminated by NFIRAOS source simulator. This DM0 pupil mask is oversized to permit using the HRWFS to view the guard actuators outside the telescope pupil beam print on the DM. Then the mask will be set to this estimated central position and the second, fine measurement and adjustment step is done.



The technique for assessing the precise centration of the IRIS Lyot mask with respect to the pupil from NFIRAOS begins by turning on the fiber sources in the NFIRAOS source simulator (Figure 5). Then a sparse poke pattern of actuators on the high-altitude-conjugated DM11, will create a non-flat wavefront, which by Fresnel propagation will turn into an easily detectable intensity pattern at a pupil. In Figure 13 on the left is the image seen by the pupil viewing camera, which results from the wavefront generated at DM11 shown on the right.[1] This array of dots on the pupil viewing camera should be concentric with the silhouette of the DM0 mask, measured in the previous step. Otherwise, fine adjustments to the mask XY position will be made.



7. CONCLUSION

A PSSN budget puts various sensitivity losses in context and permits trade-offs among them. One of the largest effects comes from an undersized Lyot mask to accommodate pupil imperfections. The procedures and equipment described in this paper effectively result in jointly calibrating residual pupil errors caused both by NFIRAOS, its interface to IRIS, and within IRIS itself. As a consequence, a Lyot mask in IRIS may be undersized by a tolerable 0.4%, thus avoiding a more conventional 1-2% undersized mask that would cause unacceptable loss of PSSN, and observing time, due to this previously underappreciated effect.

References

- [1] Véran, Jean-Pierre, Herriot, G., Telescope Pupil Tracking using a Pyramid WFS, this conference.
- [2] Seo, B-J, Nissly, C, Angeli, G, Ellerbroek, B, Nelson J, Sigrist, N, Troy, M, “Analysis of normalized point source sensitivity as a performance metric for large telescopes”, 2009, Appl. Optics, 48, 5997-6007.
- [3] Paul Hickson, “Point-Source Sensitivity for Adaptive Optics TMT.AOS.TEC.11.028, 2011-05-22
- [4] Dave Andersen, “Scientific Impact of NFIRAOS Operating Temperature” TMT.AOS.TEC.09.005
- [5] Ryuji Suzuki, “Effects of Lyot Stop on Normalized Point Source Sensitivity” TMT.INS.TEC.17.077, 2017-04-06
- [6] Glen Herriot, Pupil Shear in IRIS due to rotating IRIS' eccentric Centre of Gravity TMT.INS.TEC.16.106